MECOMARE, 14 (4) (2026) pp. 125-135

Published by: TRIGIN Publisher

International Journal of Mechanical Computational and Manufacturing Research

Journal homepage: www.trigin.pelnus.ac.id

Landslide Modeling with the Savage-Hutter Approach Using the Finite Volume Method

Brilian Prilindaputra[1], Syifa Nasiratun Toyibah[2], Dinda Rima Rachcita Putri[3], Dian Candra Rini Novitasari[4]

[1,2,3,4] Department of Mathematics, UIN Sunan Ampel Surabaya, East Java, Indonesia 60237

ARTICLE INFO

Article history:

Received Jan 30 , 2026
Revised Feb 07 , 2026
Accepted Feb 28, 2026

Keywords:

Finite Volume Method;
Landslide;
Peniraman Hill;
Savage-Hutter.

ABSTRACT

Landslides are one of the most frequent disasters in Indonesia and have a major impact on the environment and society. This study focuses on modeling the dynamics of landslides in Peniraman Hill, West Kalimantan, using the Savage-Hutter (SH) model solved through the finite volume method (FVM) and the Harten-Lax-van Leer flux scheme. (HLL), supported by the Courant–Friedrichs–Lewy (CFL) method to maintain stable conditions. This study aims to apply the model to real conditions and assess the effectiveness of the numerical approach in describing the movement of land masses. Simulations were conducted on Slopes 1 and 3 which are at risk of landslides due to their soil stability, with three variations of the soil friction angle (δ) to see how changes in these parameters affect the flow mechanism and sliding distance. The results show that the soil friction angle (δ) is a factor that influences landslide behavior. Decreasing the value δ makes the landslide move faster and cover a wider area in all parts of the topography. The initial maximum velocity of Slope 1 ranges from ~12–17 m/s with a range of around ~18 meters, while on Slope 3 it reaches ~20–27 m/s with a range of up to ~23.5 meters. Slope 3 consistently produces faster movement and longer sliding distance. Overall, the combination of the SH model with the FVM method and the HLL scheme controlled by CFL conditions has proven to be effective, stable, and capable of representing landslide dynamics. The research results can be an important basis for risk analysis and disaster mitigation strategy planning in the environment around Peniraman Hill to establish exclusion zones and design high load-bearing structures in the potential landslide reach area of ~23.5 meters.

Corresponding Author:

Dian Candra Rini Novitasari,
Department of Mathematics,
UIN Sunan Ampel Surabaya,
St. Dr. Ir. H. Soekarno No.682, Gn. Anyar, Kec. Gn. Anyar, Surabaya, East Java, Indonesia 60294.
Email: diancrini@uinsby.ac.id

1. INTRODUCTION

Landslides are one of the most frequent natural disasters in Indonesia. The combination of steep topography, high rainfall, vulnerable geological conditions, and uncontrolled human activity make landslides a serious threat (Wijaya et al., 2024). Impacts include infrastructure damage, loss of productive land, and loss of life (Wahyuzi et al., 2024).

Data from the National Disaster Management Agency (BNPB) recorded 7,024 landslides between 2015 and 2024, indicating a very high frequency of these disasters. One area prone to landslides is Peniraman Hill in West Kalimantan, where the geomorphology of the hills, soil texture

that is easily saturated with water, and the intensity of anthropogenic activity increase the slope's vulnerability to landslides, particularly during the rainy season (Ikrima et al., 2021).

Various previous studies have developed mathematical models to understand landslide phenomena. A numerical method study using the classical finite volume method to solve the 1D Savage-Hutter equations on a cohesionless avalanche of dry granular material down an inclined plane and smoothly transitioning to a horizontal plane at various angles of internal friction (Shah et al., 2024). Application of a balanced finite volume scheme to a landslide model shows close agreement with field data and estimates from the literature (Campos et al., 2023). In a study conducted by (Fan et al., 2022) the Gongjiafang landslide in the Three Gorges Reservoir was numerically simulated using a two-layer depth-averaged model and the Finite Volume Method (FVM) Harten-Lax-van Leer (HLL) scheme, the results of the study show that this model is proven to be more accurate than empirical methods in describing the series of disasters that occur due to landslides and the resulting water waves (surges). The Finite Volume method of the Savage–Hutter equations allows for conservative solutions of granular flows, while in some studies (Li & Zhang, 2020; Liu et al., 2021; Wang & Zhang, 2022) the stability of the explicit scheme is guaranteed through the application of the Courant–Friedrichs–Lewy (CFL) numerical conditions that regulate the time step size based on the maximum wave velocity of the system.

The Savage–Hutter model was selected because it can represent granular flow on steep slopes with large deformation and complex deposition, making it suitable for the field conditions in Peniraman. The finite volume method (FVM) with HLL fluxes was used for its stability in capturing shock waves and free-surface variations, with the Courant–Friedrichs–Lewy (CFL) condition controlling the time step to ensure numerical stability. Although the model has been shown to effectively describe mass-movement processes, its application in Indonesia remains limited and mostly confined to theoretical or laboratory studies (Ikrima et al., 2021). Therefore, this study applies the model with varying soil friction angles (δ) to simulate the flow mechanism and maximum landslide reach at Peniraman Hill. This study aims to provide a numerical representation of soil mass dynamics under field-like conditions and evaluate the performance of the modeling approach. The results are expected to support risk assessment and the development of mitigation strategies in landslide-prone areas.

2. RESEARCH METHOD

This study uses dynamic and numerical models to simulate landslide movement. The dynamic model is used to simulate movement over time. Meanwhile, the numerical model is used to solve the differential equations arising from the conservative model. At the conclusion of the study, a comparison will be made to determine the contribution of the parameters to the model.

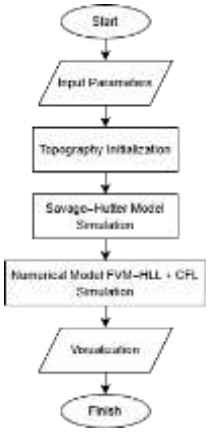

Figure 1. Flowchart of model implementation

Table 1 summarizes the overall computational framework used in this study. The implementation begins with pre-processing, followed by the application model, discretization, evaluation, and stability control.

Table 1. Computational Procedure of the Model Implementation

Phase	Mathematical Component	Numerical Method	Purpose
Pre-processing	Topography & Initial Conditions	Piecewise function	Define physical domain
Modeling	Savage–Hutter Equations	Conservative formulation	Describe mass & momentum
Discretization	Hyperbolic PDE system	Finite Volume Method	Preserve conservation
Flux Evaluation	Riemann Problem	HLL Scheme	Capture shock & discontinuity
Stability Control	Time marching	CFL condition	Ensure numerical stability
Post-processing	Height & velocity profiles	Snapshot analysis	Determine landslide reach

2.1 Scope and Assumptions

This study uses the conservative one-dimensional Savage–Hutter (SH) model to simulate landslide movement on Peniraman Hill, West Kalimantan. Data were obtained from a journal article by (Ikrima et al., 2021), which analyzed the stability of rocky soil on three slopes. This study will use data obtained from slopes 1 and 3 as parameters for running the model simulation, because data from slope 2 tests conducted by previous research is not available. The results of this study on the data from these 2 slopes are expected to be able to interpret mitigation strategies in the Peniraman Hill area.

Table 2. Input Parameters

Parameter	Slope 1	Slope 3
Slope Gradient (c)	24.7 m	30 m
Slope height (b)	16.84 m	19.28 m
Initial Slope Angle (ζ_0)	43 ^{o}	40 ^{o}
Internal Angle of Land (φ)	50 ^{o}	63 ^{o}

In addition, one soil parameter used is simplified: the cohesion value, which is assumed to indicate the mechanical properties of the slope. This method is used to maintain model simplicity while ensuring consistency of numerical calculations (Ludica et al., 2018; Wu et al., 2025). Some literature also uses an assumption for this friction angle, usually chosen $\approx \varphi$ (Ancey, 2001; Ludica et al., 2018; Shah et al., 2024; Sun & Wang, 2024). Geotechnically, this simplification can affect the geometric conditions of landslides in rock strength tests on the stress axis, the greater the friction angle value, the greater the shear strength of the soil (Ikrima et al., 2021). However, for research calibration without laboratory tests and supporting data, simulation testing was carried out:

Table 3. Soil Friction Angle Parameters

Scenario	Soil Friction Angle (δ)
1	φ
2	$\varphi - 5^{o}$
3	$\varphi - 10^{o}$

The parameters in tables 2 and 3 will also be used as values for creating topographic initialization.

2.2 Topography and Initial Conditions

Topography uses a one-dimensional slope plane with variations in slope length (L) obtained through the Pythagorean theorem based on the slope and height of the slope (Overduin & Henry, 2020), obtained:

$$L = a = \sqrt{c^2 - b^2} \#(1)$$

The slope angle $\zeta(x)$ is used as a benchmark for creating the topography. Meanwhile, the distribution of rocky soil sediments is based on the data adjusted to the domain scale, so the only difference is the slope length. This topography initialization method focuses on the effect of slope length on landslide dynamics. It prevents additional flow from outside the system, with zero boundary conditions at the ends of the domain and zero initial velocity $(u_0 = 0)$ (Ludica et al., 2018). Other factors remain constant.

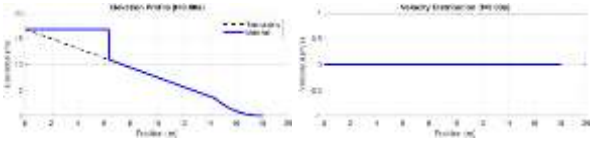

Figure 2. Initial sediment topography and distribution velocity initialization

Topography is generated using piecewise functions , dividing the domain into several intervals (subdomains). This approach is able to represent elevation variations more accurately than single functions (Bollermann et al., 2014; Fois et al., 2025). This method is also often used in contour interpolation and Digital Elevation Modeling (DEM) applications (Hutchinson, 1989; Zafar et al., 2024). The piecewise functions used in this study are:

$$\zeta(x) = \begin{cases} \zeta_0, & 0 \le x \le 0{,}8L \\ \zeta_0(1-(x-0{,}8L)/0{,}2L), & 0{,}8L < x < L \\ 0, & x \ge L \end{cases} \#(6)$$

Next, to create an inclined plane z(x)on a slope, the tangent (tan) function is used.

$$z(x) = \tan\big(\zeta(x)\big)\,(L-x) \#(7)$$

The initial sediment height initialization η(x)in this study was obtained through the following equation.

$$\eta(x) = \begin{cases} \max\big(b, z(x)\big), & x \le 0{,}35L \\ \max\big(0, z(x)\big), & \text{lainnya} \end{cases} \#(8)$$

use maxhere to satisfy the assumption that the sediment is above the topography.

2.3 Savage-Hutter (SH) Model

The Savage-Hutter (SH) model is a dynamic model used to model the movement of material flows such as landslides or dry, cohesionless granular flows, which behave like fluids. It assumes Coulomb-type basal friction with bed friction angle (δ) and Mohr–Coulomb internal behavior with internal friction angle $\varphi \ge \delta$, simplified by representing three-dimensional stress states with a single Mohr circle, so that the material density remains constant, the flow thickness is small compared to its length (shallow-flow), and the land surface has a relatively gentle curvature. This model uses a depth-averaged approach in the form of hyperbolic partial differential equations that describe the distribution of depth and average velocity of material along a defined topographic surface (Savage & Hutter, 1989). The basic model in conservative form:

$$\frac{\partial h}{\partial t} + \frac{\partial (hu)}{\partial x} = 0 \#(2)$$

$$\frac{\partial (hu)}{\partial t} + \frac{\partial}{\partial x}\left(hu^2 + \frac{1}{2}Kgh^2\cos\zeta\right) = hgS_x \#(3)$$

Equation (1) represents the continuity of mass, the change in material thickness over time determined by the mass flux of thickness and velocity. By $h(x,t)$ representing the material thickness and $u(x,t)$ landslide velocity at position xand time t. While equation (2) is for momentum conservation, including the effects of lateral material pressure (K), slope gravity (g), and basal friction (Sx).

Lateral pressure relates soil material to the angle of internal friction of the soil . There are active and passive pressures which are distinguished from the change in velocity with respect to position ($\partial u/\partial x$), if it is more than 0, then Kit is active pressure.

$$K = 2\sec^2(\varphi)\left(1 \mp \sqrt{1-\cos^2(\varphi)\sec^2(\delta)}\right) - 1 \#(4)$$

where φ is the internal angle of the soil and δ is the friction angle of the soil.

Further in the momentum equation, the gravity component drives the landslide down the slope which is influenced by the resisting movement by the basal friction angle.

$$S_x = \sin(\zeta) - \frac{u}{|u|}\tan(\delta)\cos(\zeta) \#(5)$$

where ζ is the slope angle of the topographic slope.

2.4 Finite Volume Method

The Finite Volume Method (FVM) is used to solve the conservative equations in the SH model. In the slope domain, a number of discrete cells with lengths Δx are divided as many as *N* cells, so that mass and momentum fluxes can be calculated at the boundaries of each cell. This method ensures that the conservation laws apply throughout the simulation scope (Toro, 2009). The study used a domain divided into $N = 200$ grid cells, which is commonly used in low topographic forms while still capturing sharp landslide gradients without excessive computational burden.

The conservative equation variables of the SH model are stored at the center of the cell so that their form is changed to:

$$U = \begin{bmatrix} h \\ hu \end{bmatrix} \#(9)$$

$$F(U) = \begin{bmatrix} hu \\ hu^2 + \frac{1}{2}Kgh^2\cos\zeta \end{bmatrix} \#(10)$$

$$S(U) = \begin{bmatrix} 0 \\ hg\sin\zeta - hg\cos\zeta\tan\delta\frac{u}{|u|} \end{bmatrix} \#(11)$$

so that based on equations (2) and (3) a new system of equations is obtained as:

$$\frac{\partial U}{\partial t} + \frac{\partial F(U)}{\partial x} = S(U) \#(12)$$

Next, space and time discretization is carried out in equation (8) with an integral over one control cell with a length Δx and Δt time iof n.

$$U_i^{n+1} = U_i^n - \frac{\Delta t}{\Delta x}\left(F_{i+\frac{1}{2}} - F_{i-\frac{1}{2}}\right) + \Delta t S_i^n \#(13)$$

The flux at $i + \frac{1}{2}$ is calculated from the left U_i and right U_{i+1} states using the Riemann solver Harten-Lax-van Leer (HLL). Meanwhile, the time discretization at Δt will use the Courant-Friedrichs-Lewy (CFL) condition.

2.5 Harten-Lax-van Leer (HLL) Flux

Calculating the domain, the set of cells with size Δx, and the numerical flux at each cell interface using the HLL scheme. The HLL flux is chosen because of its ability to maintain the stability of the hyperbolic solution and handle discontinuities (shocks) according to the SH model (Toro, 2019). The general HLL flux formulation is given by:

$$F_{HLL}(U_L, U_R) = \begin{cases} F(U_L), & s_L \geq 0, \\ F(U_R), & s_R \leq 0, \\ \frac{s_R F(U_L) - s_L F(U_R) + s_L s_R (U_R - U_L)}{s_R - s_L}, & \text{lainnya.} \end{cases} \#\#\#(14)$$

with $U_L$and U_R conservative variable conditions on the left and right sides of the conservative flux function cell $F(U)$, and $s_L$as well s_R as the minimum and maximum wave velocities. The estimated wave velocity limits can be written as follows.

$$s_L = \min(u_L - c_L, u_R - c_R) \#(15)$$

$$s_R = \max(u_L - c_L, u_R - c_R) \#(16)$$

with,

$$c_L = \sqrt{g h_L K_{if} \cos\zeta_{if}} \#(17)$$

$$c_R = \sqrt{g h_R K_{if} \cos\zeta_{if}} \#(18)$$

where $c_L$and $c_R$are the local wave velocities obtained from the average $Kinterface$ and the slope gradient (ζ). Thus, the HLL method was chosen because it is stable against sudden changes and can produce accurate figures (LeVeque, 2012).

2.6 Courant-Friedrichs-Lewy (CFL)

Marching time method is explicitly discretized. The CFL criterion defines a time step to ensure the scheme remains stable (Serrano-Pacheco et al., 2009):

$$\Delta t = CFL \times \frac{\Delta x}{\max_i\left(|u_i| + \sqrt{g h_i K_i \cos\zeta_i}\right)} \#(19)$$

The CFL parameter $(0 < CFL \leq 1)$regulates the balance between computation speed and stability. The value maxindicates the highest wave velocity within the domain. According to this rule, waves should not traverse more than one cell in a single time step to maintain numerical stability. Furthermore, to ensure stable simulations and convergent results, the CFL value in this study was set at 0.5 (Garres-Díaz et al., 2021; Magdalena et al., 2021)

3. RESULTS AND DISCUSSIONS

Landslide movement simulations were conducted on two slope configurations, namely Slope 1 and Slope 3. Numerical implementations used the *Savage–Hutter model* in conservative form with the finite volume method (FVM) and the HLL scheme for interface flux. In this study, simulations were conducted on 3 scenarios of soil friction angle (δ) to determine their comparison. The simulation results were visualized in the form of height profiles (*surface profiles*) and velocity distributions at several snapshot times, as well as the final profile when the material stops.

At t = 0 s, the material is at the initial height η_0 (16.84 m for Slope 1 and 19.28 m for Slope 3). The material is placed in the upstream 35% of the domain, while the rest is empty as shown in Figure 2 with a zero velocity distribution as in figure 3.

3.1 Slope Snapshot 1

The dynamic response of Slope 1 is strongly influenced by the soil friction angle parameter (δ), which causes a gradual transition of flow mechanisms. Negative values in the momentum equation indicate friction greater than gravity, resulting in a slowing of the flow. The SH formula in scenario 1 is obtained by calculating the lateral pressure,

$K = 2\sec^2(50°)\left(1 \mp \sqrt{1 - \cos^2(50°)\sec^2(50°)}\right) - 1 \approx 3{,}8405$

with left (L) and right states (R) at $h_L = 5, h_R = 1{,}5$and $u_L = 5, u_R = 1{,}5$, respectively:

$U_L = \begin{bmatrix} 5 \\ 5 \times 5 \end{bmatrix} = \begin{bmatrix} 5 \\ 25 \end{bmatrix}$

$F_L = \begin{bmatrix} 5 \times 5 \\ 5 \cdot 5^2 + \frac{1}{2} \cdot 3{,}8405 \cdot 9{,}81.5^2 \cos 43° \end{bmatrix} = \begin{bmatrix} 25 \\ 469{,}4 \end{bmatrix}$

$U_R = \begin{bmatrix} 1{,}5 \\ 1{,}5 \times 1{,}5 \end{bmatrix} = \begin{bmatrix} 1{,}5 \\ 2{,}25 \end{bmatrix}$

$F_R = \begin{bmatrix} 1{,}5 \times 1{,}5 \\ 1{,}5 \cdot 1{,}5^2 + \frac{1}{2} \cdot 3{,}8405 \cdot 9{,}81.1{,}5^2 \cos 43° \end{bmatrix} = \begin{bmatrix} 2{,}25 \\ 34{,}2 \end{bmatrix}$

and right (c_R)wave speeds are obtained (c_L),

$c_L = \sqrt{9{,}81 \cdot 5 \cdot 3{,}8405 \cdot \cos(43°)} \approx 11{,}73\ \mathrm{m/s}$

$c_R = \sqrt{9{,}81 \cdot 1{,}5 \cdot 3{,}8405 \cdot \cos(43°)} \approx 6{,}42\ \mathrm{m/s}$

so that the minimum and maximum wave speed estimates,

$S_L = \min(5.0 - 11{,}73, 1.5 - 6{,}42) = \min(-6.73, -4{,}92) = -6.73$

$S_R = \max(5.0 + 11{,}73, 1.5 + 6{,}42) = \max(16.73, 7{,}92) = 16.73$

then based on equation (14) we get

$F_{HLL} \approx 35{,}271\ \mathrm{m^2/s}$

Next, the momentum equation is calculated(S_x)
$(S_x) = 5 \cdot 9{,}81 \ \sin 43° - 5 \cdot 9{,}81 \cos 43° \ \tan 50° \cdot 1 = -9{,}2996$
The flux calculation continues to be updated conservatively using equation (13) with a discrete-time approach in equation (19). This also applies to model scenarios 2 and 3.

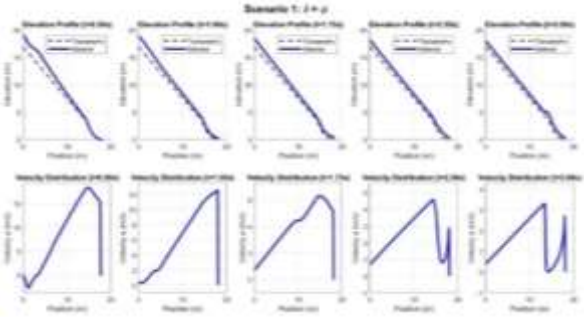

Figure 4. Height profile of slope snapshot 1 scenario 1

In scenario 1, the landslide movement is dominated by deformation of the internal friction angle of the soil (φ), as evidenced by a smooth, almost linear velocity distribution with the landslide flow on the fast-moving surface (Figure 4).

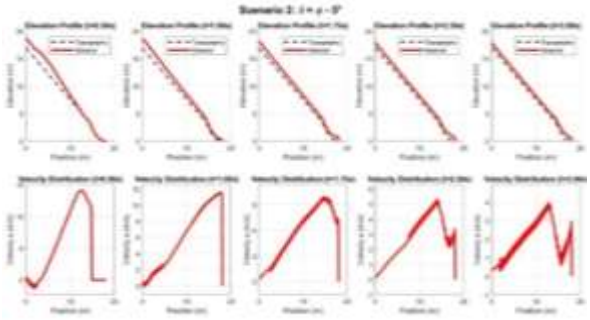

Figure 5. Height profile of slope snapshot 1 scenario 2

As base friction decreases in scenario 2, the basal sliding mechanism *becomes* active, characterized by the appearance of clear velocity oscillations and an increase in extent, especially at the base of the topography (Figure 5).

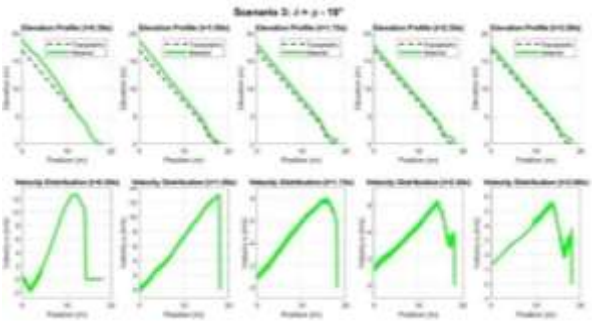

Figure 6. Height profile of slope snapshot 1 scenario 3

In scenario 3, base sliding dominates completely, resulting in the fastest flow across the topography, the longest extent, and the thinnest material distribution (Figure 6).

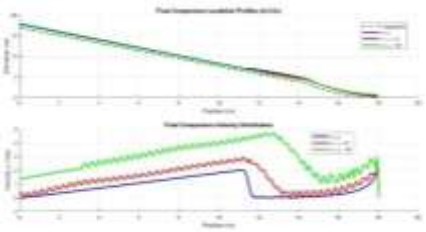

Figure 7. Final profile of slope 1 landslide

Comparison of the final conditions at t=3.5s shows that the material in all scenarios still has residual velocity, especially in scenario 3, indicating continued movement. Figure 7 also supports the finding that scenario 3 exhibits the farthest landslide reach, resulting in high mobility. Meanwhile, in the final velocity distribution, scenario 1 has the lowest velocity, approaching zero over most of the topography.

3.2 Slope Snapshot 3

Slope 3 shows a more dramatic response to changes in base friction (δ). The large negative value in the momentum equation indicates greater friction than gravity, resulting in a slowing of the flow. The SH formula in scenario 1 is obtained by calculating the lateral pressure,

$K = 2\sec^2(63°)\left(1 \mp \sqrt{1 - \cos^2(63°)\sec^2(63°)}\right) - 1 \approx 8{,}7036$

with left $(L)$and right states (R)at $h_L = 5, h_R = 1{,}5$and $u_L = 5, u_R = 1{,}5$, respectively:

$$U_L = \begin{bmatrix} 5 \\ 5 \times 5 \end{bmatrix} = \begin{bmatrix} 5 \\ 25 \end{bmatrix}$$

$$F_L = \begin{bmatrix} 5 \times 5 \\ 5 \cdot 5^2 + \frac{1}{2} \cdot 8{,}7036 \cdot 9{,}81 . 5^2 \cos 40° \end{bmatrix} = \begin{bmatrix} 25 \\ 942{,}5 \end{bmatrix}$$

$$U_R = \begin{bmatrix} 1{,}5 \\ 1{,}5 \times 1{,}5 \end{bmatrix} = \begin{bmatrix} 1{,}5 \\ 2{,}25 \end{bmatrix}$$

$$F_R = \begin{bmatrix} 1{,}5 \times 1{,}5 \\ 1{,}5 \cdot 1{,}5^2 + \frac{1}{2} \cdot 8{,}7036 \cdot 9{,}81 . 1{,}5^2 \cos 40° \end{bmatrix} = \begin{bmatrix} 2{,}25 \\ 76{,}9 \end{bmatrix}$$

and right (c_R)wave speeds are obtained (c_L),

$c_L = \sqrt{9{,}81 \cdot 5 \cdot 8{,}7036 \cdot \cos(40°)} \approx 18{,}08 \text{ m/s}$

$c_R = \sqrt{9{,}81 \cdot 1{,}5 \cdot 8{,}7036 \cdot \cos(40°)} \approx 9{,}90 \text{ m/s}$

so that the minimum and maximum wave speed estimates,

$S_L = \min(5.0 - 18{,}08\,, 1.5 - 9{,}90) = \min(-13{,}08, -8{,}40) = -13.08$

$S_R = \max\min(5.0 + 18{,}08\,, 1.5 + 9{,}90) = \max(23{,}08, 11{,}40) = 23{,}08$

then based on equation (14) we get

$F_{HLL} \approx 45{,}99 \text{ m}^2/\text{s}$

Next, the momentum equation is calculated(S_x)

$(S_x) = 5 \cdot 9{,}81 \ \sin 40° - 5 \cdot 9{,}81 \cos 40° \ \tan 63° \cdot 1 = -42{,}21$

The flux calculation continues *to be updated* conservatively using equation (13) with a discrete-time approach in equation (19). This also applies to model scenarios 2 and 3.

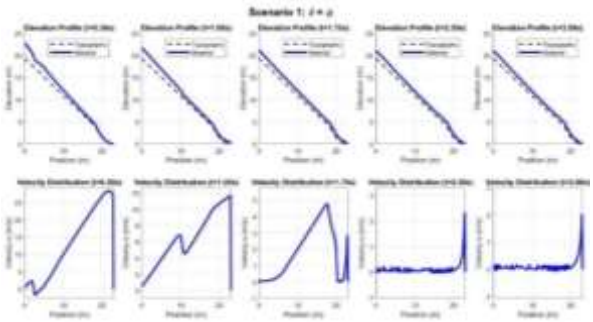

Figure 8. Slope snapshot elevation profile 3 scenario 1

In scenario 1, the landslide moves through the deformation of the internal friction angle (φ), exhibiting a very smooth velocity in the initial stage, but stabilizing and coming to a complete stop very quickly at t less than 2.5 s (Figure 8).

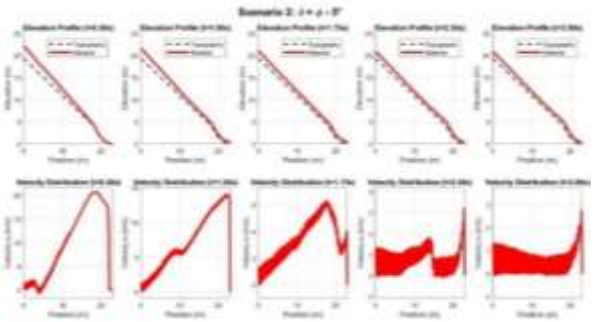

Figure 9. Height profile of slope snapshot 3 scenario 2

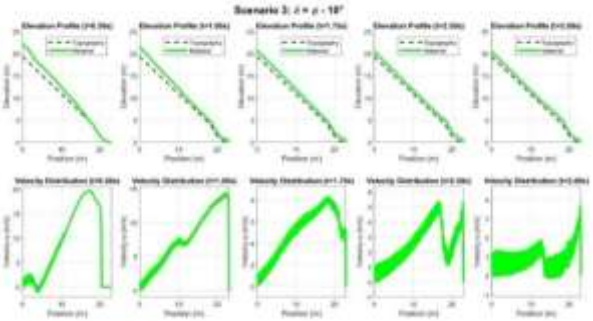

Figure 10. Slope snapshot elevation profile 3 scenario 3

This contrasts sharply with the other two scenarios. Once the base friction is reduced (Scenarios 2 and 3), the flow mechanism changes completely to a highly unstable basal sliding. This is characterized by a highly fluctuating (noisy) velocity profile*, indicating* turbulent flow (Figures 9 and 10).

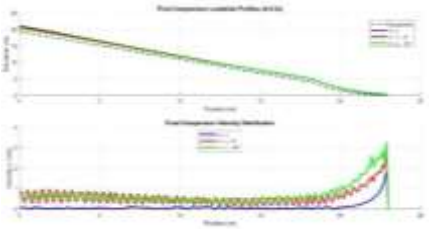

Figure 11. Final profile slope

Consequently, in both scenarios, the landslide has high mobility, a much longer reach, and does not reach a steady state even after 3.5 s (Figure 11).

3.3 Parameter Analysis

A direct comparison between Slope 1 and Slope 3 shows that initial topography influences the effect of the base friction parameter (δ). In the high-friction condition (Scenario 1), Slope 1 moves slowly in a creeping manner, while Slope 3 stabilizes more quickly. Under low friction, both slopes are dominated by basal slip, but Slope 3 exhibits more turbulent flow, whereas Slope 1 shows more regular oscillations.

The base friction parameter (δ) also controls slope sensitivity to instability. Slope 3 is more responsive to reductions in friction, with a much greater difference between rapid-stopping and long-sliding scenarios compared to Slope 1. It consistently produces longer run-out distances and thinner, more widespread deposits, indicating that accurate estimation of δ is crucial for hazard prediction, especially on steeper topographies like Slope 3, as summarized in Table 4.

Table 4. Final Results Comparison of Landslide Movement

Scenario	Maximum Velocity (m/s)		Final Reach (m)	
	Slope 1	Slope 3	Slope 1	Slope 3
1 ($\delta = \varphi$)	~17.0	~27.0	~16.5	~21.0
2 ($\delta = \varphi - 5^{o}$)	~14.0	~21.0	~17.5	~22.0
3 ($\delta = \varphi - 10^{o}$)	~12.0	~20.0	~18.0	~23.5

The research results can be an important basis for risk analysis and disaster mitigation strategy planning in the environment around Peniraman Hill to establish exclusion zones and design high load-bearing structures in the potential landslide reach area.

4. CONCLUSION

The results show that the soil friction angle (δ) is a significant factor influencing landslide behavior. Decreasing the value δ causes landslides to move faster and cover a wider area across all topographical sections, although the initial velocity decreases slightly. On Slope 1, the reach increases from approximately ~16.5 m to ~18 m, while on Slope 3 it increases from approximately ~21 m to ~23.5 m with higher velocities overall. Topographic differences also influence the simulation results, with Slope 3 showing greater sensitivity to changes in friction parameters compared to Slope 1.

Overall, the combination of the FVM method and the HLL flux scheme proved effective, stable, and capable of realistically depicting landflow dynamics according to field conditions in Indonesia. These findings contribute to landslide risk analysis and mitigation through numerical simulation. However, the model is limited to a one-dimensional (1D) approach that does not capture lateral mass dispersion, and the soil friction parameter (δ) remains uncertain due to the absence of laboratory validation. Future research should extend the model to higher dimensions and incorporate cohesion and additional factors to improve predictive accuracy.

REFERENCES

Ancey, C. (2001). Dry Granular Flows Down An Inclined Channel: Experimental Investigations On The Frictional-Collisional Regime. *Phys. Rev. E*, *65*(1), 11304. https://doi.org/10.1103/PhysRevE.65.011304

Bollermann, A., Chen, G., Kurganov, A., & Noelle, S. (2013). A Well-Balanced Reconstruction of Wet/Dry Fronts for the Shallow Water Equations. *J. Sci. Comput.*, *56*(2), 267–290. https://doi.org/10.1007/s10915-012-9677-5

Campos, F., Sepúlveda, M., Abarca, R., & Issler, D. (2023). Study of Avalanche Models Using Well-Balanced Finite Volume Schemes. *Obras y Proyectos*, *63*, 54–63. https://doi.org/doi.org/10.21703/0718-281320233306

Fan, Y., Ma, D., & Sun, X. (2022). Numerical Investigation of the Landslide and Its Surge: A Case Study of the Gongjiafang Landslide in the Three Gorges Reservoir Area. *Geofluids*, *2022*, 13. https://doi.org/10.1155/2022/3800053

Fois, M., Gatti, F., de Falco, C., & Formaggia, L. (2025). A Comparative Analysis of Mesh-Based and Particle-Based Numerical Methods for Landslide Run-Out Simulations. *Computers & Fluids*, *295*, 106641. https://doi.org/https://doi.org/10.1016/j.compfluid.2025.106641

Garres-Díaz, J., Fernández-Nieto, E. D., Mangeney, A., & Morales de Luna, T. (2021). A Weakly Non-hydrostatic Shallow Model for Dry Granular Flows. *Journal of Scientific Computing*, *86*(2), 25. https://doi.org/10.1007/s10915-020-01377-9

Hutchinson, M. F. (1989). A New Procedure for Gridding Elevation and Stream Line Data with Automatic Removal of Spurious Pits. *Journal of Hydrology*, *106*(3), 211–232. https://doi.org/https://doi.org/10.1016/0022-1694(89)90073-5

Ikrima, U., Purwoko, B., & Syafrianto, M. K. (2021). Analisa Kestabilan Lereng pada Bukit Peniraman dengan Menggunakan Metode Stereografis. *JeLAST : Jurnal Teknik Kelautan , PWK , Sipil, Dan Tambang*, *8*(2), 1–9. https://doi.org/10.26418/jelast.v8i2.49427

LeVeque, R. J. (2012). *Finite Volume Methods and Software for Hyperbolic Problems*. NSF Award. 16732. https://ui.adsabs.harvard.edu/abs/2012nsf

Li, R., & Zhang, X. (2020). A Finite Volume Scheme for Savage-Hutter Equations on Unstructured Grids. *Numerical Mathematics*, *13*(2), 479–496. https://doi.org/10.4208/NMTMA.OA-2019-0080

Liu, W., Hu, Y., He, S., Zhou, J., & Chen, K. (2021). A Numerical Study of the Critical Threshold for Landslide Dam Formation Considering Landslide and River Dynamics. *Frontiers in Earth Science*, *9*(May), 1–11. https://doi.org/10.3389/feart.2021.651887

Ludica, Alifanda Pinkan Gunawan, P. H., & Rohmawati, A. A. (2018). Simulasi Pergerakan Runtuhan Longsor Menggunakan Model Savage-Hutter Dengan Finite Volume Method. *E-Jurnal Matematika*, *7*(2), 88. https://doi.org/10.24843/mtk.2018.v07.i02.p189

Magdalena, I., Hariz, A. A. A., Farid, M., & Kusuma, M. S. B. (2021). Numerical Studies Using Staggered Finite Volume For Dam Break Flow With An Obstacle Through Different Geometries. *Results in Applied Mathematics*, *12*. https://doi.org/10.1016/j.rinam.2021.100193

Overduin, J., & Henry, R. C. (2020). *Physics and the Pythagorean Theorem*. 1–10. http://arxiv.org/abs/2005.10671

Savage, S. B., & Hutter, K. (1989). The Motion Of A Finite Mass Of Granular Material Down A Rough Incline. *Journal of Fluid Mechanics*, *199*(2697), 177–215. https://doi.org/10.1017/S0022112089000340

Serrano-Pacheco, A., Murillo, J., & García-Navarro, P. (2009). A Finite Volume Method For The Simulation Of The Waves Generated By Landslides. *Journal of Hydrology*, *373*(3–4), 273–289. https://doi.org/https://doi.org/10.1016/j.jhydrol.2009.05.003

Shah, A., Zafar, M. N., Du, Y., & Yuan, L. (2024). *Numerical Solution of the Savage – Hutter Equations for Granular Avalanche Flow using the Discontinuous Galerkin Method*. https://doi.org/doi.org/10.48550/arXiv.2205.05161

Sun, W., & Wang, Y. (2024). Modeling Phase Separation in Grain-Fluid Mixture Flows by a Depth-Averaged Approach With Dilatancy Effects. *Journal of Geophysical Research: Earth Surface*, *129*(12). https://doi.org/https://doi.org/10.1029/2023JF007416

Toro, E. F. (2009). *Riemann Solvers And Numerical Methods For Fluid Dynamics: A Practical Introduction*. https://doi.org/10.1007/b79761

Toro, E. F. (2019). The HLLC Riemann solver. *Shock Waves*, *29*. https://doi.org/10.1007/s00193-019-00912-4

Wahyuzi, R., Muslim, D., Zakaria, Z., Sukiyah, E., & Sophian, R. I. (2024). Potensi Longsor Akibat Aktivitas Penambangan Ilegal di Kecamatan Sungai Durian, Kabupaten Kotabaru. *Jurnal Teknologi Mineral Dan Batubara*, *20*(2), 65–76. https://doi.org/10.30556/jtmb.vol20.no2.2024.1567

Wang, M., & Zhang, X. (2022). A High – Order WENO Scheme Based on Different Numerical Fluxes for the Savage – Hutter Equations. *Mathematics*, *10*(1482), 1–18. https://doi.org/doi.org/10.3390/math10091482

Wijaya, A. H., Fajriyanto, Novianti, T. C., & Rahmadi, E. (2024). Pemetaan Daerah Bahaya Tanah Longsor Di Kecamatan Balik Bukit Kabupaten Lampung Barat Dengan Metode Weighted Overlay. *Journal Of Plano Studies*, *1*(2), 62–71. https://doi.org/10.36982/jops.v1i2.4904

Wu, Y., Wang, Z., Zhao, Y., Li, X., & Wang, Y. (2025). Flow-pile interaction for landslides: Fluid simulation model. *Journal of Rock Mechanics and Geotechnical Engineering*. https://doi.org/ttps://doi.org/10.1016/j.jrmge.2025.05.009.

Zafar, M. N., Dutykh, D., Sabatier, P., Banjan, M., & Kim, J. (2024). Numerical Reconstruction of Landslide Paleotsunami Using Geological Records in Alpine Lake Aiguebelette. *Journal of Geophysical Research: Solid Earth*, *129*(5), e2023JB028629. https://doi.org/https://doi.org/10.1029/2023JB028629